Nationaal Lucht- en Ruimtevaartlaboratorium
National Aerospace Laboratory NLR

Executive Summary

A study of grid convergence issues for the simulation of the massively separated flow around a stalled airfoil using DES and related methods

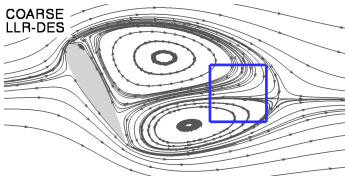

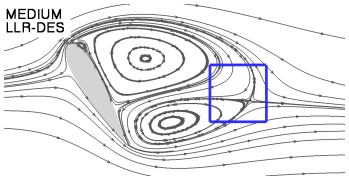

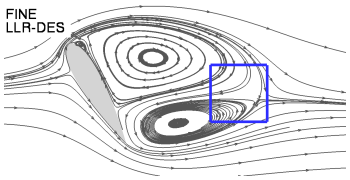

Problem area
Time-dependent flow phenomena can have a strong impact on performance and flight characteristics of aerospace vehicles and therefore play a crucial role in their design and operation. On modern high-performance fighter aircraft well-ordered leading-edge vortices are deliberately generated. Under specific operational conditions, the vortices break down and lose their well-ordered structure. As a result, highly dynamic flow can be impinging on downstream tail structural components, which may cause early fatigue or loss of the tail structure. In other cases, vortex breakdown is an important factor leading to uncommanded oscillatory motions of fighter aircraft, such as nose slice, wing rock and wing drop. For space launchers, an important challenge is to accurately assess dynamic external loads on the structural components of the space launcher, caused by massively separated flow. For passenger aircraft, the noise generated by the landing gear is caused by the turbulent eddies separating from the landing gear, again leading to strong pressure fluctuations.

Efforts to simulate the flows mentioned above and the associated dynamics based on the Reynolds-Averaged Navier-Stokes (RANS) equations have revealed several problems. For separated flows, the frequency range of the dominant flow structures cannot be discriminated from the turbulence spectrum, a basic assumption of RANS simulations. Moreover, the RANS equations incorporate too much dissipation in the flow separation areas to resolve small scales. On the other hand, Large Eddy Simulation (LES) for realistic geometries and Reynolds numbers is years off due to the inherently large computational complexity as a result of the resolution required close to solid boundaries.

Report no.
NLR-TP-2006-436

Author(s)
K.A. Weinman, H. van der Ven, C.R. Mockett, T.A. Knopp, J.C. Kok, R.T.E. Perrin and F.H. Thiele

Classification report
Unclassified

Date
September 2006

Knowledge area(s)
Computational Physics en Theoretische Aërodynamica

Descriptor(s)
hybrid RANS-LES
massively separated flow
grid convergence
DES
X-LES

This paper is accepted for presentation at the ECCOMAS CFD 2006 conference, September, 5-8, 2006, Egmond aan Zee.

Hybrid methods, based on a combination of RANS and LES modelling, in principle can relieve the computational characteristics of LES, and at the same time improve the RANS turbulence modelling capabilities. Basically, a RANS turbulence model is applied near the geometry, and an LES turbulence model is applied in the wake. Where a realistic LES simulation requires top-of-the-bill supercomputers, hybrid RANS-LES simulations are in principle feasible on current compute servers, although they are computationally much more demanding that RANS computations, as both good temporal and spatial resolution of the separated flow areas are necessary.

Description of work

In a joint effort, DLR, TU-Berlin, and NLR have started a grid convergence study for hybrid RANS-LES simulations of a stalled airfoil. The expected outcome of the study are criteria for mesh generation for such simulations, which are independent of differences in physical modeling, numerical algorithms and implementation details. In addition to the statements made on grid convergence, the paper also summarises the practical aspects of conducting such a grid convergence study, that is, the computational burden, as well as reviewing the various post-processing techniques employed to provide recommendations for others wishing to conduct such a study.

Results and conclusions

Concerning the integral force coefficient prediction and time-averaged flow topology, the effect of grid refinement has been seen to be strong for all partners. The different analysis techniques used to examine the flow in the wake however have shown largely the same flow features, as well as similar trends with grid refinement. The extent to which each method allows the issuing of concrete verdicts concerning grid convergence can however first be determined once additional data has been computed on the finest grids, which is the subject of ongoing work. The computational expense of the study turned out to be considerable, primarily due to the necessity of simulating a very large number of time steps for statistical convergence.

Applicability

Hybrid RANS-LES methods are designed to simulate massively separated flows at relevantly increased accuracy (compared to RANS) and significantly reduced computational costs (compared to LES). Massively separated flows occur in many aerodynamic applications:

- Vortex breakdown for fighter aircraft,
- Weapon bay acoustics,
- Store separation,
- Landing gear acoustics,
- High-lift configurations for passenger aircraft,
- Rotorcraft flow,
- Base flow space launchers, missiles, flares, etc.
- Jet noise,
- Buffeting/LCO.

The method shows qualitatively good results, which are strong incentives to continue development. In order to obtain reliable quantitative results, the grid dependency and the interface between the RANS and LES require attention.

Nationaal Lucht- en Ruimtevaartlaboratorium, National Aerospace Laboratory NLR

Anthony Fokkerweg 2, 1059 CM Amsterdam,
P.O. Box 90502, 1006 BM Amsterdam, The Netherlands
Telephone +31 20 511 31 13, Fax +31 20 511 32 10, Web site: www.nlr.nl

Nationaal Lucht- en Ruimtevaartlaboratorium
National Aerospace Laboratory NLR

NLR-TP-2006-436

A study of grid convergence issues for the simulation of the massively separated flow around a stalled airfoil using DES and related methods

K.A. Weinman[1], H. van der Ven, C.R. Mockett[2], T.A.Knopp[1], J.C. Kok, R.T.E. Perrin[2] and F.H. Thiele[2]

1 German Aerospace Laboratory DLR
2 Technical University Berlin

This report is based on a presentation to be held at the ECCOMAS CFD 2006 conference, Egmond aan Zee, The Netherlands, September 5-8, 2006.

Customer	National Aerospace Laboratory NLR
Contract number	----
Owner	National Aerospace Laboratory NLR
Division	Aerospace Vehicles
Distribution	Unlimited
Classification of title	Unclassified
	September 2006

Approved by:

Author	Reviewer	Managing department
25/9/2006	25/9/06	25/9/'06

Summary

A systematic grid convergence study is conducted for the Detached-Eddy Simulation (DES) of the massively separated flow around a NACA0021 airfoil at high angle of attack. In order to study the convergence characteristics of DES/LES problems, velocity fields using a series of grids must be generated that demonstrate sufficient dynamic similarity to allow the assumption that the physics encapsulated within the solutions are similar. It is then possible to examine which characteristics of the fields can be used as indicators of some measure of grid convergence. The work detailed in this paper describes the methods that have been used to assess the level of convergence obtained on three grids by three partners using variations of the DES method implemented in different numerical solvers. In addition to recommendations on the methods employed for grid convergence assessment, information is provided concerning the computational expense and industrial feasibility of such studies. As an interesting secondary issue, the study provides opportunity for the direct cross-comparison of models and codes.

Contents

4 Tables
12 Figures

(34 pages in total)

List of figures

This page is intentionally left blank.

1 Introduction

Since its conception (Ref. 16), the Detached-Eddy Simulation (DES) method has become an increasingly applied tool for the treatment of certain classes of turbulent flows in engineering fluid mechanics. The reason for this is primarily the ability to combine the advantages and eliminate the disadvantages of URANS and LES techniques through a relatively simple modification to an existing RANS model. DES has been shown to be considerably advantageous to URANS methods for a range of flows featuring highly unsteady, massively separated flow (Ref. 4, 20), whilst reducing the numerical cost compared to fully-resolved LES through the treatment of the attached turbulent boundary layers using RANS. In successive works, the method has been generalised to a formulation applicable to any one-equation or two-equation RANS model (Ref. 21), and a derivative approach known as X-LES involving an additional substitution of the length scale switch has also been developed (Ref. 8).

Despite this relative success, a number of open questions remain to be addressed, many of which concern the development of the DES concept to a mature method for industrial application. As with all CFD methods, one of the most important of these issues is that of numerical grid resolution, in particular the derivation of relevant best practice guidelines. The principle source of information on the design of grids for DES was issued by Spalart in 2001 (Ref. 17). This describes very clearly the necessary multi-zonal approach, and the general requirements for the various grid regions. In particular, the near-wake region of massively separated flow behind a bluff body, referred to as the "focus region" (Ref. 17) must satisfy the resolution requirements of LES. However, Spalart also acknowledges that concrete and generally-applicable criteria for the resolution of LES in separated flow regions is lacking (as opposed to criteria for the LES of wall-bounded flows, which are generally well-defined in terms of normalised wall-units). The only guideline given in this respect, is that the focus region grid must be successively refined until a grid-convergent solution is obtained (Ref. 17). Furthermore, the grid refinement must be conducted in all three dimensions, using a constant refinement factor (a minimum of $\sqrt{2}$ was suggested). A precursor study by Mockett et al. (Ref. 10) did indeed suggest the presence of a strong dependency of DES on the resolution of the near-wake region behind a stalled airfoil. However, no generally-applicable conclusions could be drawn from this study as the grid refinement was not conducted systematically, and the computations were limited to a single CFD code. To the authors' best knowledge, no such systematic grid refinement study has yet been published for DES, and it was to address these important issues that the current investigation was launched.

In the standard DES approach, the filter width is a function of the mesh width. As the grid is refined more turbulence scales are resolved and a conventional numerical grid convergence study

cannot be performed. In order to avoid this problem, all DES models employed in this paper apply a constant filter width which remains constant regardless of the mesh resolution, so the same physical problem is solved on all meshes. Apart from allowing a grid convergence study, a fixed filter width also circumvents some of the more intricate problems of LES modelling such as non-commutivity of the filtering operator with spatial differentiation. It is worth noting that for quasi-2D geometries such airfoils, the usual definition of the filter width is often determined by the constant spanwise resolution.

As the philosophy of LES is based on the resolution of the majority of the turbulent kinetic energy, and modelling of the smallest scales, an investigation of the range of scales present in the solution at each grid level is important. An attempt has therefore been made to extend the type of post-processing typical for RANS investigations (time-averaged integral force coefficients etc.) to a range of methods which deal with the unsteady content of the flow. Furthermore, the in-house CFD algorithms of three separate institutions are tested collaboratively, and each algorithm uses DES or a related approach implemented to different RANS models. The intention is hereby to ensure that any conclusions made concern DES as a method and are not code, implementation or model-specific. The institutions concerned are the German Aerospace Centre, the National Aerospace Laboratory of the Netherlands, and the Technical University of Berlin, which shall be referred to in the following as DLR, NLR and TUB respectively. In addition to the statements made on grid convergence, the paper also summarises the practical aspects of conducting such a grid convergence study, i.e. the computational burden, as well as reviewing the various post-processing techniques employed to provide recommendations for others wishing to conduct such a study.

2 Method

2.1 Plan of Work

In order to confidently obtain some estimates that are appropriate in the measurement of a LES/DES grid convergence metric, it is first necessary to generate set of flow fields which are, in some measure yet to be defined, within a convergence range similar to that of the asymptotic convergence range often used in more conventional RANS studies. In order to select a suitable set of fields for further study the following points were considered.

Test case: The case chosen for the grid convergence study was the massively separated flow around a NACA0021 airfoil at 60° angle of attack and a Reynolds number of 270000, chosen due to the availability of time-resolved experimental force data (Ref. 19). To limit

the computational expense, a periodic spanwise domain of one chord length c is used. Guenot (Ref. 3) computed a similar test case, the NACA0012 airfoil at 45° angle of attack and Re 100000, using DES and a range of periodic spanwise domain sizes (whilst keeping the spanwise resolution constant). This investigation showed a strong dependency of the mean forces on the spanwise domain, which renders the direct comparison of these quantities with the experimental data invalid. Therefore, the evaluation is based on the degree of asymptotic convergence with grid refinement, not with respect to agreement with experimental values.

Multiple partners/models/codes: The use of several different codes is intended to facilitate conclusions which are independent of model, algorithm, and implementation details.

Grids: Three grids are employed, between which a constant refinement ratio of 1.5 exists in all three spatial directions. The grid was designed to concentrate points into the "focus region" of the near wake, maintaining a resolution as uniform as possible, whilst providing approximately cubic cell dimensions as required for LES (Ref. 17). This results in 4.77×10^5, 1.59×10^6 and 5.32×10^6 nodes for the coarse, medium and fine grids respectively. The span direction is resolved with 32, 48 and 72 grid cells in the coarse, medium and fine grid respectively. Figure 1 shows a slice normal to the spanwise direction for the medium grid. It should be noted that to date only one partner has been able to compute a sufficient data series on the finest mesh. The reference coordinate system is shown in Figure 2; x in the streamwise direction, y in the spanwise direcion and z in the vertical direction.

Time step: The time step has been chosen on a Courant-Friedrichs-Levy criterion based on the fine grid requirements. A uniform time step was chosen on all meshes in order to avoid additional considerations relating to the numerical error associated with the time discretisation.

Fixed filter width: By fixing the filter width, the same physical problem is solved on all three meshes, which is a necessary prerequisite for grid convergence studies (see Section 2.2 for details).

Selection of data capture region: Figure 2 illustrates the test section of the flow within which the detailed study was undertaken. The field at every time step was saved in this three-dimensional box, which was chosen to study the LES region of the flow whilst minimising data storage requirements. Several analytical methods have been used in this work, including phase averaging, time averaging, proper orthogonal decomposition methods as well as some spectral estimations in wavenumber space. Time averaging is well understood and will not be discussed here, with the exception that the number of samples required to obtain even statistically converged first and second order moments require excessive computational effort. The other post processing methods applied are discussed in sections 2.6

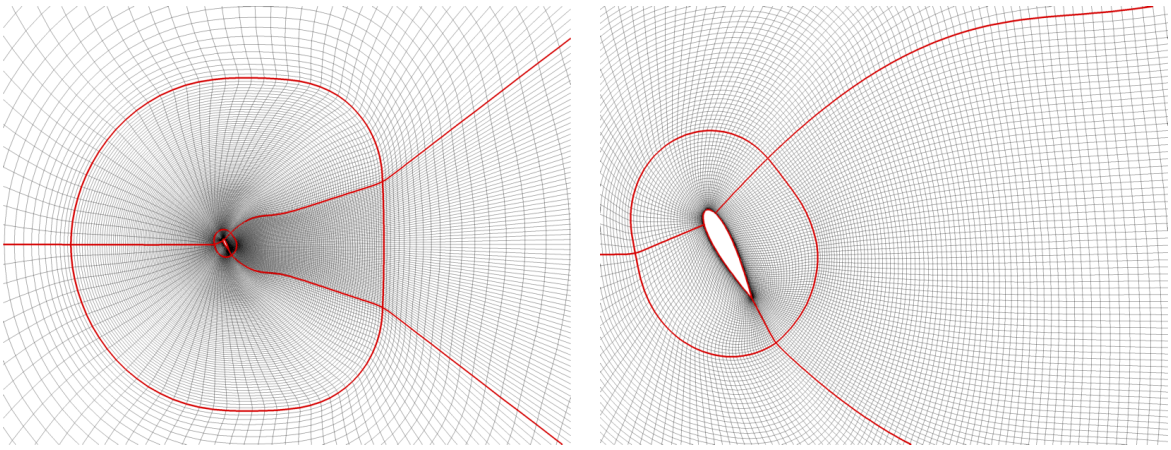

Fig. 1 x/z plane of medium grid: zoomout view of topology left, detail around profile right

and 2.7.

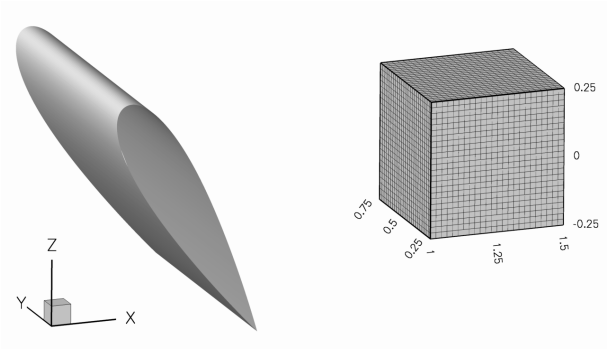

Fig. 2 Schematic of geometry, coordinate system and box location (medium grid resolution shown), incidental flow in positive x-direction

2.2 Treatment of the filter width Δ

The hybrid nature of DES leads to a complicated situation when grid convergence behaviour is considered, which is dominated by the LES-mode region of the flow. Unlike RANS methods, grid refinement past a point of convergence will not deliver the same solution. Rather, as the grid scale decreases, so does the LES filter width until the limit case of a fully-resolved DNS is reached. In order to address this problem, a fixed model filter width Δ_f is introduced, which is kept constant as the grid resolution is varied. As the resolution in the focus region is coarsest in the spanwise direction, the standard DES filter width, $\Delta_{DES} = max[\Delta_x, \Delta_y, \Delta_z]$, would return a width of $c/32$ on the coarse grid. The value of Δ_f is therefore chosen as $c/32$. Whereas NLR and DLR have implemented $\Delta = \Delta_f$ throughout the entire domain, TUB uses $\Delta = max[\Delta_f, \Delta_{DES}]$ to ensure that the filter width does not become smaller than the grid spacing in regions of coarser mesh (e.g. in the far wake). The influence that this difference will have on

the computed results is assumed to be small. Through the introduction of Δ_f, the subgrid scale model behaviour remains constant while the spatial resolution is refined. Thus the additional terms due to the LES part of the models remain fixed functions of the filter width, so that grid convergence behaviour should be observed.

2.3 DLR Tau flow solver and SA-DDES implementation

The DLR TAU code (Ref. 13) is a finite volume unstructured method, which solves the Reynolds Averaged Navier-Stokes equations on a cell-vertex metrics. The code is used to solve both steady and unsteady problems, and both dual time stepping and global time stepping are supported for the latter. Explicit and implicit solution algorithms have been implemented, based on well-known Runge-Kutta methods for explicit calculations and a LU-SGS method (Ref. 2) for implicit calculations. The inviscid flux terms can be treated with either central, upwind or hybrid (Ref. 21) schemes. Either matrix or scalar dissipation is used to stabilise the convective central difference operators. Viscous terms are treated using a conventional central differencing scheme. Additional low Mach number preconditioning may be used to maintain numerical efficiency in incompressible flow regimes. Several variations of the Spalart-Allmaras turbulence model, the Wilcox two equation model and RSM models have been implemented into the code.

The calculations presented in this work have been obtained using dual time stepping with the LU-SGS solver on the dual grid metric. Previous work with the Tau code in DES calculations has relied upon the scalar dissipation model, however the matrix dissipation model has been tested during the course of this project, and has been found to provide some improvement in the resolution of fine-scale structures when compared to the scalar dissipation results. The DES model presented in this work is the "delayed DES" (DDES) variant of the Spalart-Allmaras DES due to Spalart et al. (Ref. 18). Further details regarding the DDES model and the Tau code may be found in the above references. It should be noted that a value of $C_{DES} = 0.45$ was used in the calculations on the basis of calibration using the decay of isotropic turbulence (DIT).

2.4 NLR ENSOLV flow solver and X-LES implementation

The flow solver ENSOLV, which is part of NLR's multi-block flow simulation system ENFLOW, models compressible, turbulent flows with the Reynolds-averaged Navier–Stokes equations or with the X-LES approach. The X-LES formulation (Ref. 8) consists of a composition of the TNT k–ω model and a k-equation subgrid-scale model. The composite length scale

$$\tilde{l} = \min\{\sqrt{k}/\omega, C_1\Delta\} \tag{1}$$

(with Δ the filter width and the X-LES constant $C_1 = 0.05$, obtained via calibration against the decay of isotropic turbulence) is used in the expressions for the eddy viscosity and for the

dissipation of turbulent kinetic energy, i.e.

$$\nu_t = \tilde{l}\sqrt{k} \qquad \text{and} \qquad \varepsilon = \beta_k \frac{k^{3/2}}{\tilde{l}}. \tag{2}$$

The flow equations are discretised in space by a cell-centred, finite-volume method, using multi-block structured grids, central differences, matrix-type artificial diffusion for the basic flow equations and a second-order TVD treatment of convective terms in the k–ω equations (Ref. 7). In LES mode, a high-order discretisation of the convective operator is required. A new high-order finite-volume method (Ref. 9) is used, which is based on the skew-symmetric form of the convective operator, has low numerical dispersion and dissipation, and is fourth-order accurate on non-uniform, smooth curvilinear grids. Using the skew-symmetric form leads to conservation of kinetic energy by the convective operator which enhances numerical stability and avoids interference with the dissipation of kinetic energy due to the sub-grid scale model. The equations are integrated in time by a second-order implicit scheme. Per time step, the non-linear equations are solved by a multi-grid scheme that uses Runge–Kutta pseudo-time integration as relaxation operator combined with a line-implicit scheme to deal with grid cells of high aspect ratio. To maintain the efficiency and accuracy for weakly compressible flows, low-Mach preconditioning is applied, following Turkel (Ref. 22).

2.5 TUB ELAN code and LLR-DES implementation

ELAN is the in-house finite-volume development code of TU-Berlin, and has been in use for around 10 years. The code solves the Navier-Stokes equations in either a steady or unsteady context, and employs RANS and LES for turbulence treatment. The procedure is implicit and of second order accuracy in space and time (Ref. 23), with variables stored in the cell centres of curvilinear, block-structured grids. Diffusive terms are approximated with central schemes, whereas convective terms can be treated with central or upwind-biased limited schemes of higher order. A hybrid blending of both approaches is used for Detached-Eddy Simulation as suggested by Travin et al. (Ref. 21), the goal of which is to address the antagonistic requirements of the RANS and LES zones on the convection scheme via localised blending between central or upwind schemes. The pressure is obtained using a pressure-correction scheme of the SIMPLE type, which assures mass conservation (Ref. 6), and a generalised Rhie and Chow interpolation is used (Ref. 11).

A range of turbulence models are available in *ELAN*, and the DES modification has been implemented to many of these. The model chosen for the current investigation is the Linear Local

Realizable (LLR) $k-\omega$ model (Ref. 12), which is a local linear two-parameter model derived from realizability and non-equilibrium turbulence constraints. The DES length scale

$$L_{DES} = min[L_{RANS}, C_{DES}\Delta] \tag{3}$$

is substituted in place of the model turbulence length scale, L_{RANS} in the destruction term of the k transport equation, where

$$L_{RANS} = \frac{k^{1/2}}{C_\mu \omega} \quad . \tag{4}$$

A value of $C_{DES} = 0.75$ is used, which is obtained from calibration against decaying isotropic turbulence (DIT) (Ref. 1).

2.6 Phase averaging technique

The bluff body wake flow exhibits large-scale, von-Karman style vortex shedding, which is quasi-periodic in nature. Accordingly, the flow can be considered in the framework of a triple decomposition into a mean flow plus coherent and incoherent fluctuations, representing the vortex street motion and the broadband fluid turbulence, respectively. Such a decomposition should allow comparison of the trajectories of the large-scale vortices predicted on each grid and between each partner, as well as an assessment of the resolution of turbulent fluctuations convected with these. For each simulated time step the corresponding phase angle of vortex shedding must be determined, on the basis of which a conditional averaging can be conducted. To determine the phase angle, the tangential force coefficient C_t is taken as a trigger signal. This is particularly suitable, as it exhibits a dominant periodic character and very low levels of higher-frequency noise, as can be seen in Figure 3. To remove any residual high-frequency components, a band-pass filter is applied, before the phase angle is determined using a Hilbert transformation and the local maxima and minima of the filtered signal. As can be seen in Figure 3, the period of each phase can vary quite considerably. The fixing of the zero and $\pi/2$ phase angle at local minima and maxima adds additional accuracy in respect of this modulation.

Each shedding period is divided into 16 phase angles, which are then linked to the corresponding computational time step. In this study, phase averaging has been applied both to the unsteady box fields and the spatial energy spectra of the box data.

2.7 Proper orthogonal decomposition method

In order to study coherent structures in the dynamic flow, a Karhunen-Loéve expansion is performed on the computed fields. This expansion is also known as the proper orthogonal decomposition (POD) method. First an orthogonal decomposition of the velocity field $u(x,t)$ is computed

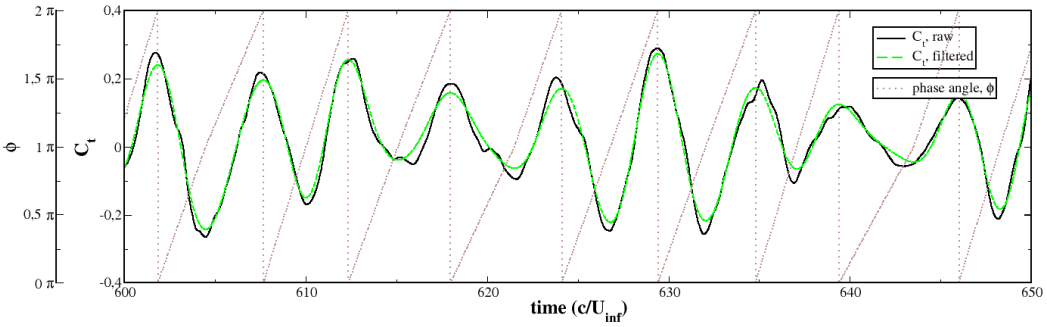

Fig. 3 Time trace of tangential force coefficient C_t, raw and filtered, and the phase angle ϕ derived from the latter

such that the field can be written

$$u(x,t) = \sum_{n=1}^{\infty} a_n(t)\varphi_n(x), \tag{5}$$

where the $\{\varphi_n(x); n = 1, 2 \cdots\}$ are a set of real orthonormal basis functions and the a_n are the basis function coefficients, which are random. An important feature of the definition of the POD is that the basis functions are chosen to maximise the energy contained within modes. The basis functions are then given by the solution of the eigenvalue problem for the integral equation containing the two point velocity correlation as its kernel.

In this paper the snapshot POD proposed by Sirovich (Ref. 14) is applied. Assuming that the number of grid points under consideration is N, for the standard POD an eigenvalue problem of size N must be solved. The snapshot POD solves the eigenvalue problem for the discretised coefficients $a_n^k = a_n(t_k), k = 1, \ldots, M$ in the POD expansion. In this way, the size of the eigenvalue problem becomes M, with M being the number of snapshots taken from the time series chosen so that $M \ll N$. However, the snapshots must be statistically independent and the optimal method for reconstructing the two point velocity correlation tensor from the snapshot data is not known. The method is therefore dependent on how the M snapshots are chosen. All POD analyses in this paper have been performed with the DLR INVEST package.

2.8 Computational expense

Table 1 presents computational requirements as observed by the partners involved in these computations. The entry 'Flop count per time step per grid cell' provides the number of floating point operations to advance the flow in one grid cell by one time step. The flop counts for DLR and TUB are estimated from an expected sustained performance of 10% of the peak performance

Code	TAU		ENSOLV		ELAN		
Model	SA-DDES		XLES		LLR		
Grid	coarse	medium	coarse	medium	coarse	medium	fine
Number of processors	4	12	1	3	8	10	32
Number of inner its.	100	100	20	30	14	14	14
time/it. (secs)	1.58	1.72	8.75	6.45	4.32	11.66	8.55
(est.) kflop count (/step/cell)	530	520	370	552	-	-	547
time for 25000 time steps (days)	45	50	50	56	18	47	35

Table 1 Estimates of computational requirements as observed by partners computing test cases.DLR uses an AMD Opteron Cluster (peak performance per processor 4 Gflop/s), NLR an NEC SX-5 (8 Gflop/s) and TUB use Intel Pentium 4 clusters, and the IBM p690 system (7.6 Gflop/s) of the HLRN for the fine grid (see acknowledgments).

of the system. Despite the difference in the numerical schemes, the computational complexity of the simulations are comparable. It is clear from the table that this type of grid convergence study could at present not be adopted as routine practice in an industrial context, even if the coarse mesh solution could be considered of sufficient resolution for engineering accuracy. The computational expense is dominated by the required number of time steps, and not by the spatial resolution. It should be noted, however, that the number of time steps required for statistical convergence strongly depends on the application. It is known that for this application, high levels of modulation at frequencies much lower than that of the vortex shedding are apparent (Ref. 10, 19), which may be due to slightly different natural shedding frequencies at the leading and trailing edges. As a result, the number of time steps required is very high for this application.

3 Discussion of results

3.1 Integral force coefficients and shedding frequency

Table 2 presents a comparison of the integral force coefficients and characteristic shedding frequency (Strouhal number, St) returned by the different computations. Examination of the table shows that the frequency information embedded within each time series is quite similar, whereas larger differences are apparent in the values of the integral force coefficients.

As observed in section 2.1, an agreement of the computed integral values with experiment is not expected as the spanwise domain used in these calculations is one chord length, in comparison

Model	Grid	C_l	$(\sigma/\mu)_{C_l}$	C_d	$(\sigma/\mu)_{C_d}$	C_l/C_d	St	Samp.size
SA-DDES	Coarse	0.95	0.17	1.47	0.15	0.646	0.19	16952
SA-DDES	Medium	0.91	0.20	1.50	0.21	0.607	0.18	14283
SA-DDES	Fine	-	-	-	-	-	-	-
X-LES	Coarse	1.09	0.20	1.58	0.18	0.690	0.19	12550
X-LES	Medium	1.15	0.22	1.71	0.18	0.673	0.18	11250
X-LES	Fine	-	-	-	-	-	-	-
LLR-DES	Coarse	0.96	0.18	1.55	0.17	0.619	0.18	63381
LLR-DES	Medium	1.09	0.24	1.83	0.19	0.596	0.18	31566
LLR-DES	Fine	1.04	0.22	1.74	0.19	0.598	0.18	42000

Table 2 Estimates of integral parameters obtained for all partners and grids. Experimentally-obtained values (Ref. 19) of lift and drag are $C_l = 0.93$ and $C_d = 1.55$.

to the value of between four and five found by Guenot (Ref. 3) to provide converged integral values. The X-LES and LLR-DES calculations show similar trends as the grid is refined from the coarse to the medium mesh, with an increase in both the lift and drag values. For the SA-DDES model, however, the drag increases whilst the lift decreases. This suggests that different unsteady dynamics are present in the two-equation and one-equation models, both in the boundary layer as well as in the wake regions of the flow. Despite the significant differences in lift and drag observed, the computed ratios of root mean square (σ) to mean (μ) of these quantities remain comparable. The unsteady variation in both lift and drag is therefore thought to be only weakly dependent on turbulence model and grid, which supports the observation concerning the returned Strouhal number. It is important to note that the LLR-DES model, for which solutions on three grids have been computed, does not return an indication of asymptotic convergence. Unfortunately, the fine grid solutions for the X-LES and SA-DDES are required before further discussion can be conducted concerning this matter.

3.2 Time-averaged flow field

Having examined the integral force coefficients and Strouhal numbers obtained from the various calculations, the time-averaged flow field shall now be investigated. Reynolds averaging was conducted concurrently with the calculations for the total number of time steps stated in Table 2, with the exception of the SA-DDES medium grid computations, where a lower number of time steps (7000) than that used to obtain the integral forces was available. In the cases of the SA-DDES and LLR-DES computations, additional averaging was conducted in the homogeneous spanwise direction. The time-averaged streamlines are displayed in Figure 4, together with an

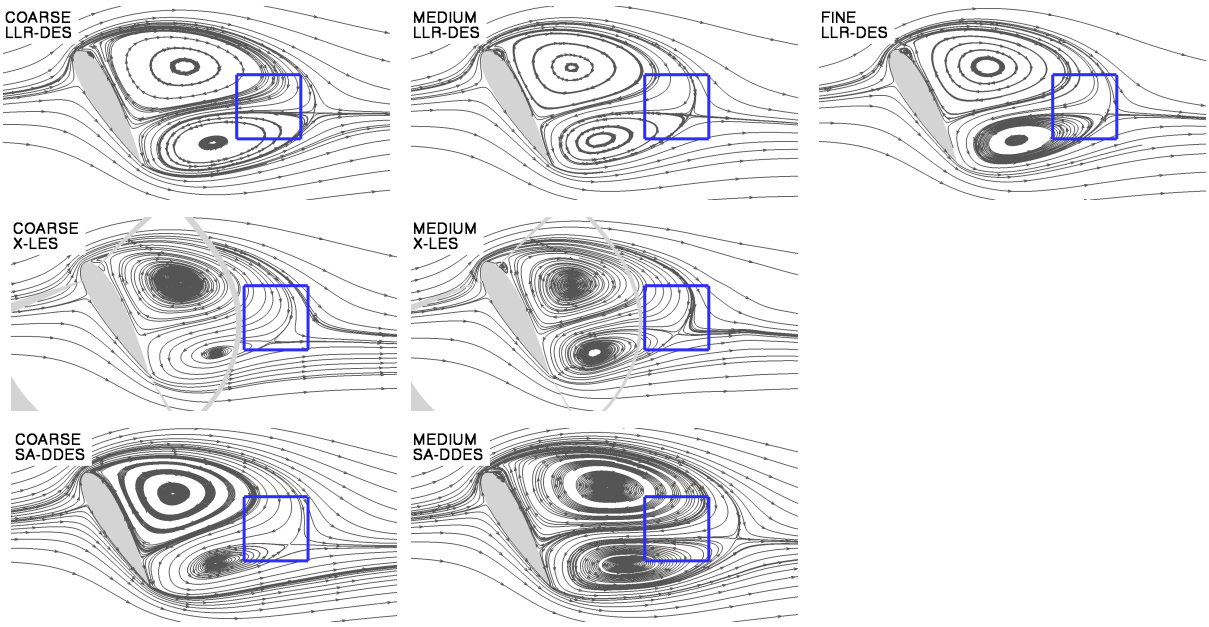

Fig. 4 Time and spanwise-averaged streamlines showing location of the topological features, all partners and grids.

outline of the sampling box location for reference. The basic topology of two large recirculation regions is returned by all calculations, although a level of difference can be observed in the length of the wake and the positions of the leading and trailing edge vortex centres.

Under initial inspection, it can be seen that the agreement between both two-equation models (X-LES and LLR-DES) is relatively high, whereas the one-equation SA-DDES results appear to return a longer time-averaged recirculation region. It must be emphasised that different CFD-solvers are used with each model, so comparative calculations using the same solver would be necessary before valid conclusions concerning the model influence could be made.

Closer examination of the locations of the vortex cores (with their associated pressure minima) reveals the commonality between partner results as well as a correlation with the integral force coefficient values in Table 2. Looking firstly at the fields returned on the coarse and medium mesh by all partners, it can be seen that in all cases the trailing edge vortex moves closer to the rear surface of the airfoil as the mesh is refined. This may be due to an enhanced breakdown of the trailing edge shear layer into resolved turbulent structures enabled by the finer mesh. Differences between the partner results emerge when the movement of the leading edge vortex with mesh refinement is considered, which is towards the airfoil for the LLR-DES and X-LES results, and away from the airfoil in the case of SA-DDES. The trend for the SA-DDES result is influenced by a topological difference in the coarse mesh field; the secondary separation as the recir-

culating flow approaches the leading edge apparent in all other fields is not reproduced. It was observed in section 3.1 that the trends for lift and drag between grids are reversed for the SA-DDES results. This may be influenced by the difference in the relative proximities of the leading and trailing edge vortices seen between the two grids for SA-DDES. Furthermore, a correlation between the ratio of the distances of the two vortices and the lift-to-drag ratio for each grid (Table 2) can be seen for all models. For the computations in which the relative vortex positions do not change strongly between grids, and for which the development of the lift and drag coincide (i.e. LLR-DES and X-LES), a correlation between the proximity of the vortices and levels of the integral forces is apparent.

The Reynolds averaged resolved kinetic energy, $\overline{k_{res}}$ is plotted in Figure 5, where $\overline{k_{res}} = \frac{1}{2}\overline{u_i u_i}$ with $\overline{u_i u_i}$ obtained statistically from the resolved velocity field neglecting modelled contributions. In all computations, the peak levels of $\overline{k_{res}}$ are found near the centre of the trailing edge vortex. The peak values obtained follow the same trend as the integral forces for the LLR-DES and X-LES results, and the peak levels on the SA-DDES medium grid results are also higher than the coarse grid. This is in line with expectation, as when the grid is refined, more scales are resolved and the level of the resolved turbulent kinetic energy should rise accordingly.

An idea of the levels of modelled turbulence activity can be obtained from Figure 6, where the time-averaged values of the turbulent to molecular viscosity ratio, $\overline{\nu_t/\nu}$ from the LLR-DES and X-LES computations are shown. It is important to note that due to the different background RANS models used by the partners, quantitative agreement between partner computations is not to be expected, rather the trend between grid levels it to be compared. Very interestingly, this trend appears to be reversed for the LLR-DES and X-LES computations, with values of $\overline{\nu_t/\nu}$ in the near-wake focus region decaying with increasing grid refinement for the LLR-DES results, and increasing for the X-LES results. Furthermore, for the LLR-DES computations the values increase considerably as the grid coarsens in the departure and far wake regions. For the X-LES computations, the values drop to near freestream levels. Two key differences exist between the LLR-DES and X-LES implementations. Firstly, as noted in Section 2.4, the X-LES formulation employs an additional substition of the DES length scale in the expression for the eddy viscosity. Furthermore, as described in Section 2.2, the implementation of the fixed filter width Δ_f is different for the LLR-DES and X-LES algorithms. As the grid coarsens in the far wake region, the X-LES filter width remains equal to Δ_f, meaning that the subgrid model essentially becomes inactive, and numerical diffusion arising due to the coarser grid dominates. Despite this difference, the mean flow fields (Figure 4) and trend in integral forces (Table 2) are very similar.

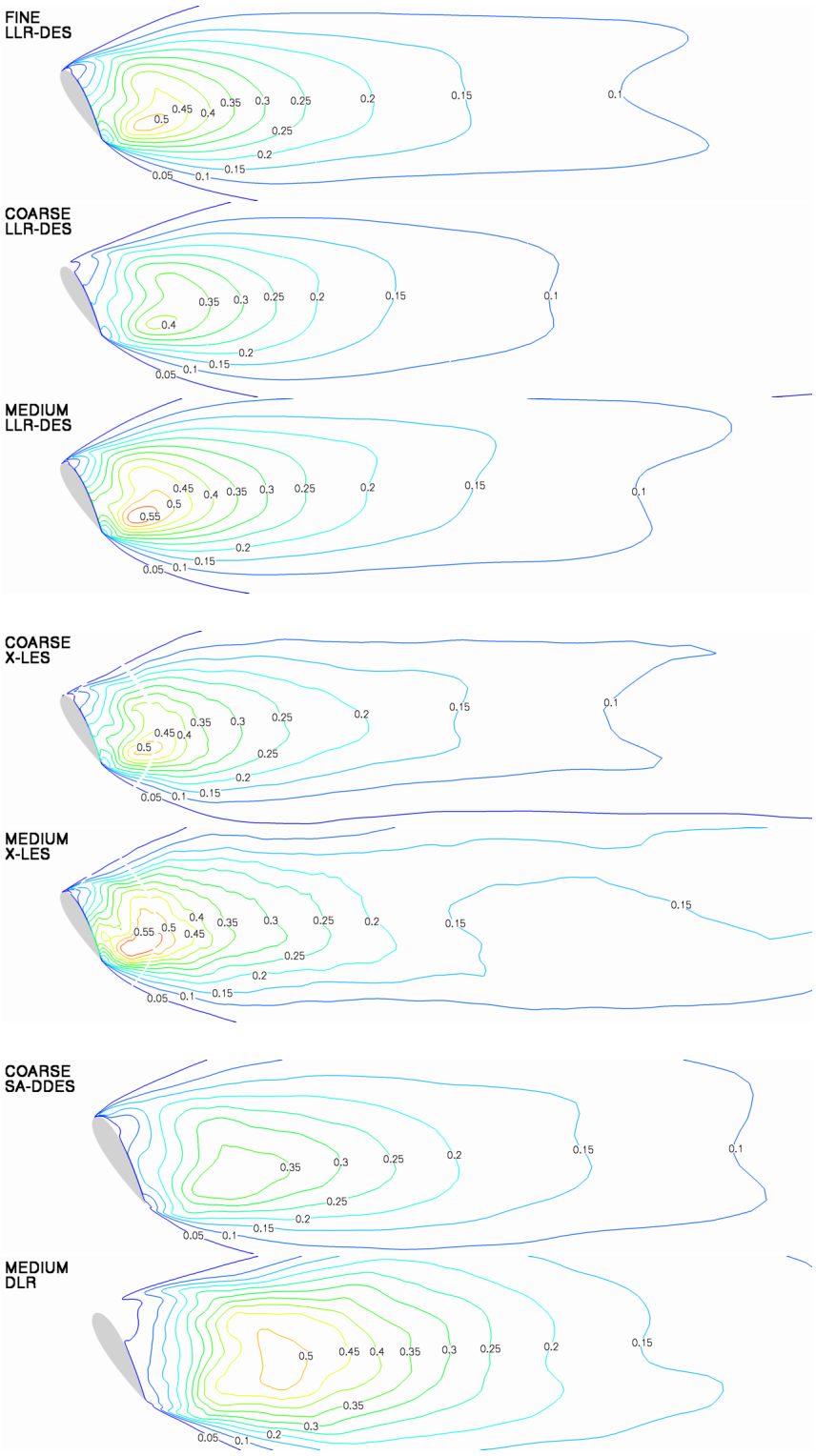

Fig. 5 Resolved kinetic energy of Reynolds-averaged field $\overline{k_{res}}$, all partners and grids

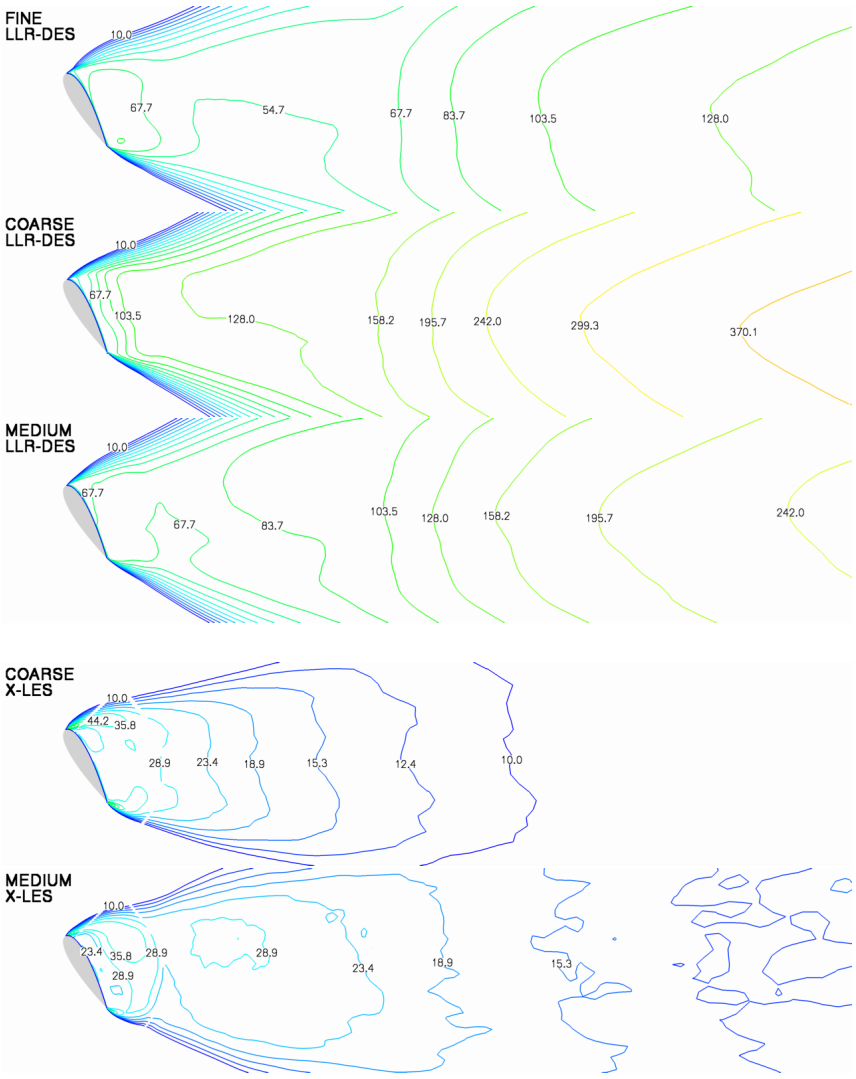

Fig. 6 Reynolds-averaged eddy viscosity ratio $\overline{\nu_t/\nu}$, all grids, LLR-DES and X-LES

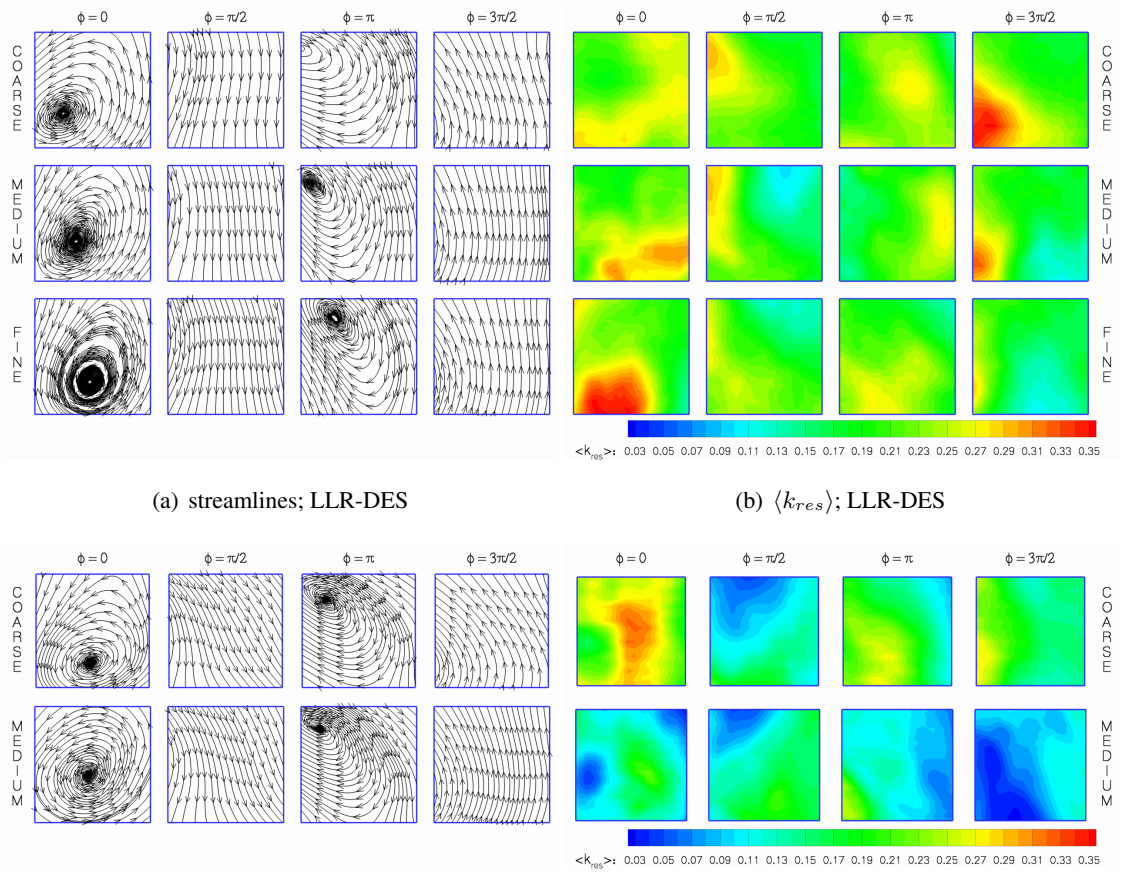

(a) streamlines; LLR-DES

(b) $\langle k_{res} \rangle$; LLR-DES

(c) streamlines; X-LES

(d) $\langle k_{res} \rangle$; X-LES

Fig. 7 Phase-averaged flow fields showing streamlines the phase-averaged velocity $\langle U_i \rangle$ for all grids (left) and resolved turbulence kinetic energy of fluctuations away from the phase-averaged flow , $\langle k_{res} \rangle$ for all grids (right). The phase angle $\phi = 0, \frac{\pi}{2}, \pi, \frac{3\pi}{2}$ varies horizontally, the meshes vertically from coarse to fine.

3.3 Phase-averaged flow field

Using the method described in Section 2.6, the unsteady data sampled in the box region was phase-averaged in an attempt to separate the large scale coherent motion of the vortex shedding from the small-scale turbulent fluctuations. Figures 7(a) and 7(c) show the streamlines of the phase-averaged flow field, $\langle U_i \rangle$ from the LLR-DES and X-LES computations respectively. The basic traversal of the box region by the leading and trailing edge vortices are captured similarly by both sets of simulations. However, a trend is seen in the LLR-DES data between coarse, medium and fine grids, whereby the location of the vortices at each phase angle is successively shifted rearwards. In contrast, the coarse and medium X-LES results do not indicate this trend, and the leading edge vortex is even further forward for the medium grid at $\phi = \pi$.

The resolved kinetic energy fluctuations away from the phase-averaged flow, $\langle k_{res} \rangle$ are shown in Figures 7(b) and 7(d) for the LLR-DES and X-LES computations respectively. The peak values appear to be located in the shear regions between the vortices in all cases. Whereas a trend of increasing $\langle k_{res} \rangle$ can be seen in the LLR-DES results, the opposite is true for the X-LES results, in contrast to the total $\overline{k_{res}}$ obtained by Reynolds averaging (Figure 5). This suggests that the coherent contribution to $\overline{k_{res}}$ is greater, and the incoherent contribution less for the X-LES computations compared to the LLR-DES results. However, it must be borne in mind that the phase-averaging of second moment statistics places very high demands on statistical convergence, and this hypothesis is to be treated with caution.

3.4 Spatial spectral content

The velocity field in the box can be analysed for its spectral content, comparable to the analysis of the energy spectra in decaying isotropic (homogeneous) turbulence. For the box in the wake, however, the flow is neither isotropic, nor periodic. In order to prevent contamination of the Fourier signal with the discontinuities at the box boundaries, a Hanning window is applied. The result is a time series of energy spectra. The spectra may then be averaged in time, but it is more interesting to apply the phase averaging procedure of Section 2.6. The X-LES and LLR-DES results are shown in Figure 8.

Overall, the different methods and meshes show the same trends, with two peaks occurring at the second wave number. All methods and meshes predict the peaks at about the same phase angles. With an increase in resolution the overall level of kinetic energy in the smaller scales increases, as expected. For the medium mesh results, the peaks at the second wave number more or less coincide with a reduction of energy content in the higher wave numbers. This is not seen in the fine mesh LLR-DES results, suggesting a higher energy content for the higher wave numbers. One would also expect more temporal dynamics in the small scales (of the size of the filter width) for the fine mesh simulation. That this does not occur may suggest that the fine scales in the box have different frequencies than the vortex shedding frequency.

3.5 Temporal spectral content

The time spectra of an individual point inside the box have been computed from the X-LES and SA-DDES results by averaging windows of 4096 and 1536 samples respectively, using the TUB tool *dftavg*. As shown in Figure 9, the vertical velocity component demonstrates a peak at the shedding frequency of St=0.2. Although also visible in the streamwise component (not shown here), this peak is strongest for the vertical velocity component, as would be expected. The pressure coefficient signal shows a second peak at St=0.4. The trends between the two meshes are the

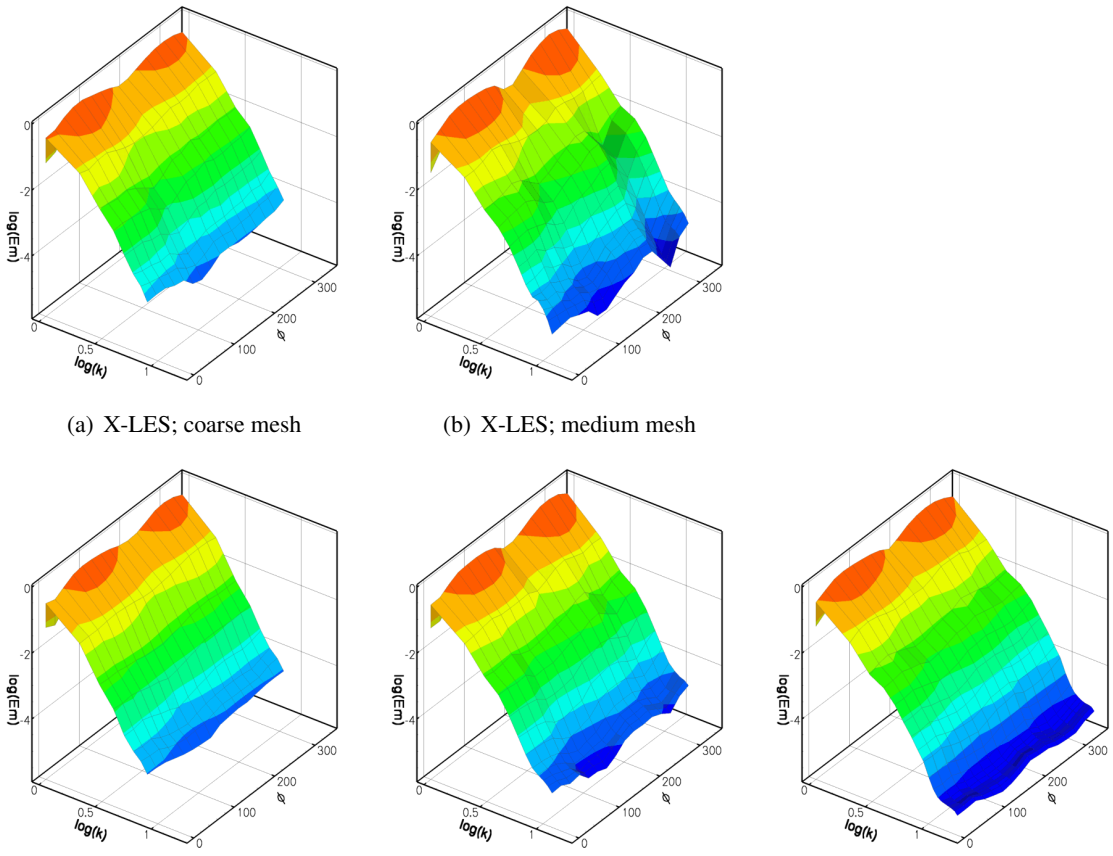

(a) X-LES; coarse mesh (b) X-LES; medium mesh

(c) LLR-DES; coarse mesh (d) LLR-DES; medium mesh (e) LLR-DES; fine mesh

Fig. 8 Phase-averaged energy spectra in the box. In the figures, k is the spatial wave number, ϕ the phase angle, and Em *the kinetic energy.*

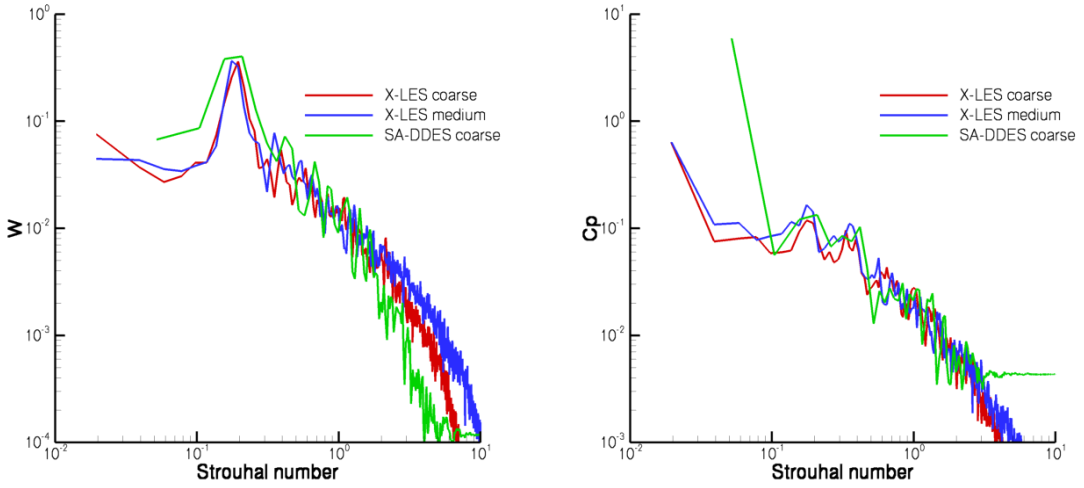

(a) Vertical velocity component

(b) Pressure coefficient

Fig. 9 Temporal spectra of vertical velocity component and pressure coefficient in a probe in the box

same, with the medium mesh showing higher amplitudes at higher frequencies, indicating higher levels of resolved turbulence.

The spectra compare very well between partners, and it is expected that the principle differences are caused by the variations in sampling length.

3.6 Probability density functions

Examination of the probability density functions (PDF) of the flow in the test box is of interest, as this allows some characterisation of the flow fields. Figure 10(a) illustrates the probability distribution functions of the velocity components observed in the test box. The velocity distributions are compared for the X-LES model on medium and coarse grids, as well as the SA-DDES model on the coarse grid. Even though the sampling length for each model/grid combination is different, it can be seen that the behaviour is very similar between the different meshes shown, as well as for the different turbulence models tested. In Figure 4 it is seen that the box occupies a region that is jointly populated by both the upper and lower averaged vortical structures, which must have oppposite circulation. In all cases, the upper vortex directs momentum on average out of the box in the downstream direction, whilst the lower vortical structures contribute momentum in both the upstream and downstream directions. The U (streamwise) component has a positive mean, indicating a mean outflow in the dowstream direction and the domination of the upper

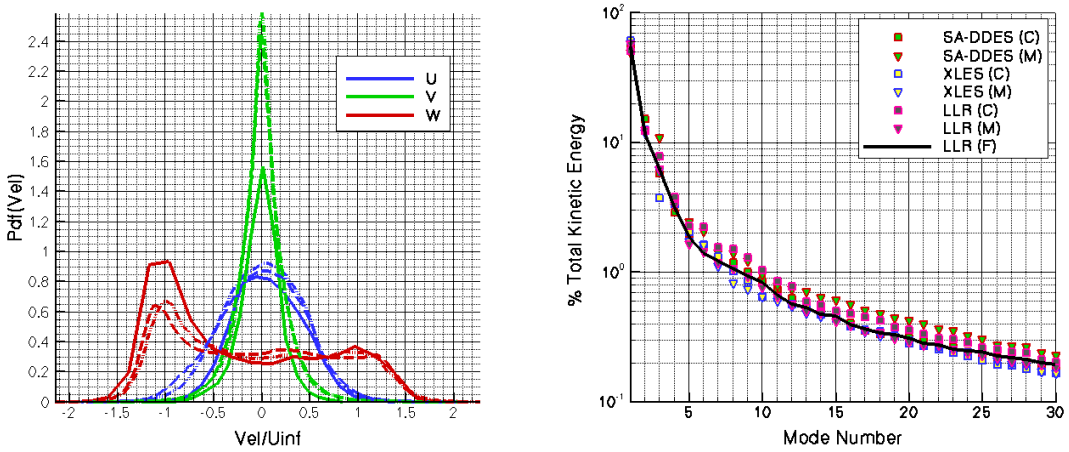

(a) Comparison of Velocity Probability Distribution function for test field.

(b) Comparison of fractional energy contribution per mode.

Fig. 10 Comparison of velocity probability density functions as well as the fractional energy contribution of the most coherent modes. Note that for (a) the solid line is obtained from the X-LES medium grid solution, while the dashed lines are from the SA-DDES and X-LES coarse grid solutions

vortex for the flow within the box. The vertical velocity component, W, is dominated by large deviations, which are due to the presence of vortices originating from the leading and trailing edges of the airfoil. However the probablitity distributions are not symmetric, with a mean downflow occuring in the box, which is due to the induced downwash caused by the trailing vortex street. The spanwise velocity component, v, is almost Gaussian with zero mean for all calculations, suggesting that little or no mean transport occurs in this direction, confirming that the flow is quasi two-dimensional. The PDF analysis suggests that the resolved structures returned for the different calculations in the test field show a significant amount of similarity. The principal differences between mesh/turbuence model combinations are strongly dependent on variations in sample length and, in contrast to the time and spanwise-averaged fields, these statistics show little influence of the grid or the turbulence model.

3.7 Proper Orthogonal Decomposition

The POD method as described in Section 2.7 has been applied to the box velocity fields. Table 3 provides an indication as to the selection of the sampling for the different calculations. The POD analysis results showed little dependency on the number of samples and how they were selected.

Model	SA-DDES		X-LES		LLR-DES		
Grid	C	M	C	M	C	M	F
Total Sample size	15100	7800	4000	4000	16740	7884	21600
Sample Interval	50	50	10	10	27	27	27
M	302	156	400	400	620	292	800

Table 3 Sample selection strategy used by different partners in implementing the Sirovich method.

Mode m	SA-DDES		XLES		LLR		
	C	M	C	M	C	M	F
1	56.21	49.46	60.84	57.8	50.9	57.3	54.8
2	15.25	11.85	12.45	19,21	12.4	12.5	11.5
3	5.77	10.90	3.72	6.16	7.8	6.3	6.3
4	2.91	3.23	3.38	3.43	3.8	3.3	3,1
5	1.97	2.46	2.03	1.72	2.3	1.6	1,9
6	1.59	2.08	1.62	1.62	2.2	1.4	1.4
7	1.53	1.43	1.31	1.11	1.55	1.2	1.2
8	1.18	1.41	1.02	0.82	1.50	1.1	1.1
9	1.00	1.23	0.86	0.74	1.30	0.93	0.93
10	0.86	0.96	0.65	0.65	1.03	0.76	0.84
$\sum_{m=1}^{10}$	88.28	85.01	87.91	86.15	84.75	86.40	83.00

Table 4 Estimates of the modal contribution to the total kinetic energy obtained for the three different models on the selected grids.

In terms of the correlation matrices

$$R_{ij} = (\varphi_i, \varphi'_j) \tag{6}$$

for two sets of basis functions, the differences due to sampling strategy were less than the differences observed due to grid or turbulence model selection.

Figure 10(b) provides a comparison of the predicted fractions of energy in each mode for all calculations presented in this paper. As noted, the distribution of energy is influenced by the strategy used in selecting the M snapshots, however the fractional energy distributions show a large amount of independence from the turbulence model and the grid used. As the grid is refined, all computations, with the exception of the LLR-DES result, show decreasing contributions from the first mode to the total energy in the test field. As the grid scale is decreased and finer scales

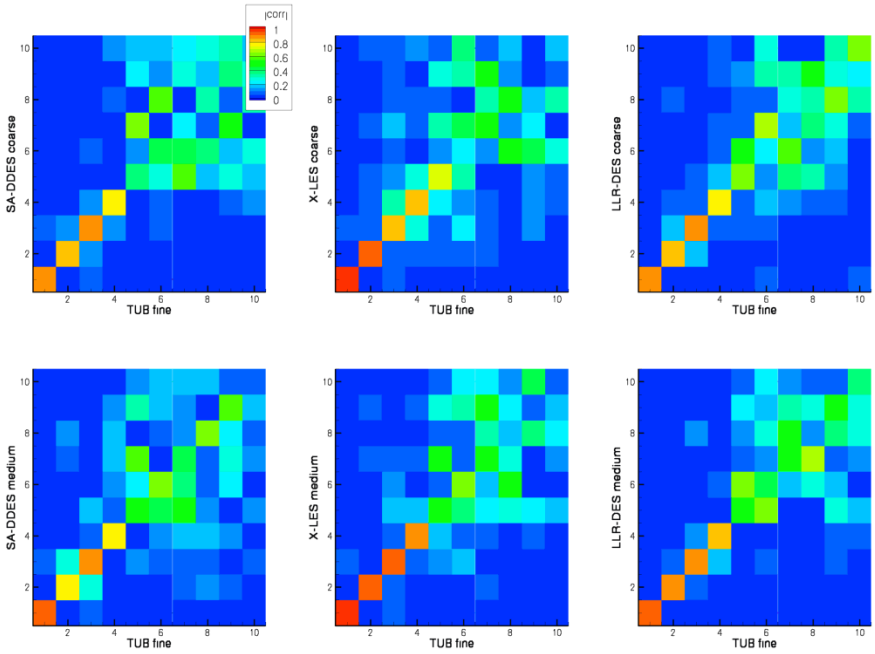

Fig. 11 Comparison of the correlation coefficients calculated from the covariance between the solution modes and the reference modes (LLR-DES fine grid).

of motion are then resolved, energy in the lowest modes is redistributed to the higher modes so that the energy cascades from lowest modes to higher modes as the level of the resolved field is increased. The LLR-DES medium grid result is in this context quite unexpected, and may indicate that the LLR-DES sub-grid scale model has slightly different dynamics to that of the other models. On the basis of the LLR-DES fine grid solution, the error norm of the fractional energy content can be estimated to lie within linear part of the convergence range (where the change in error is a linear function of the grid scale) for the LLR-DES and X-LES models. This suggests that all meshes are sufficiently well resolved for LLR-DES and X-LES methods.

3.7.1 Correlation of principal models

An additional estimate characterising the similarity of the different fields can be made by computing the correlation betwen the principal modes of the POD decomposition. It can be expected that if the most energetic modes within the solutions are very similar, the solutions are not strongly dependent on the grid or turbulence model used. In order to test the similarity of the most energetic modes, the correlation coefficient between the modes is computed using equation (6), and the computed correlations are shown in Figure 11.

While issues relating to sample size are still relevant, it can be seen that, for the most energetic modes, the degree of correlation of the coarse and medium grid solution for the different turbu-

lence models with the reference LLR-DES fine grid solution is quite high. As the order of the modes increases, the magnitude of the corelations tend to drop off. This may be due to grid convergence and turbulence model issues or weaknesses in the construction of the two-point velocity correlation function required in the POD method. However, the high correlation of the X-LES coarse and medium grid results with the LLR-DES fine grid results suggests that the problem is in the selection of the M samples required for the Sirovich method and in differences in the dynamic behaviouor of the DES models themselves. A clear trend can nonetheless be seen, in that the maximum correlation coefficient occurs on the diagonal of the plotted matrix. These figures support the assumption that the principal modes returned by the computations do not appear to be strongly influenced by the turbulence model used, however further study is needed in order to examine this point of view more closely.

For all calculations, the first four most energetic modes were very similar, and these are shown in Figure 12. The most energetic mode corresponds to a mean velocity normal to the onflow and spanwise directions. The second most energetic mode demonstrates a cylindrical topology with its axis lying along the spanwise direction. This mode is associated with the motion of the detached vortices through the test box. The third mode corresponds to a velocity direction parallel to the onflow direction and is probably a direct consequence of the continuity constraint as the first mode changes direction. The fourth mode seems do be associated with velocity components switching direction about a saddle point structure as alternate vortical shedding occurs about the airfoil leading and trailing edges. However the fourth and higher modes will suffer to some extent from an insufficient number of snapshots M, and it is difficult to state quantitative results for the higher modes. The topology of the modes returned by the POD method is similar for all calculations, however examination of Figure 4 indicates that the saddle point structure does not exist within the averaged box flow structure for the LLR-DES coarse grid results and the SA-DDES medium grid results. This suggests that the saddle point position varies significantly with time and is probably influenced by the shedding from the leading and trailing edges. Additional study is required to examine the temporal nature of such solution features.

4 Conclusion

A range of techniques for studying the grid convergence of DES-like simulation methods have been described and compared using the bluff body test case of an airfoil in deep stall. The computational expense of the study turned out to be considerable, primarily due to the necessity of simulating a very large number of time steps for statistical convergence. As such it can be concluded that although the application of DES-like methods is beginning to emerge in an industrial

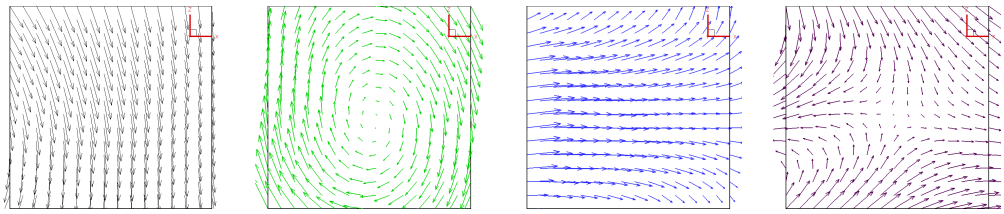

Fig. 12 First four modes obtained for the SA-DDES coarse grid solution.

context, it will be a long time before the routine application of such grid convergence studies will be feasible. Furthermore, the computational expense has served to provide the most significant source of uncertainty in this study.

Concerning the integral force coefficient prediction and time-averaged flow topology, the effect of grid refinement has been seen to be strong for all partners, with variations of up to around 15% seen in the drag coefficient and quantitative (and in one case qualitative) changes seen in the flow topology. It is worth pointing out that the level of variation is still much less than seen in a comparative study of different URANS models on the same mesh (Ref. 4). The various analyses of the unsteady flow field in the separated region has by contrast shown a high degree of similarity in the large-scale flow characteristics between partners and grids, despite an increase in the resolution of small-scale structures observed with grid refinement. It thus appears as if the separated shear layer and near-wake regions are more dominated by model, grid and implementation differences than the further separated region.

The different analysis techniques used to examine the flow in the unsteady sampling box have shown largely the same flow features, as well as similar trends with grid refinement, so can all be considered applicable in principle. However, more practical or fundamental reasons may influence the recommendation of one method over the other. The phase averaging method has been useful for examining the contributions of coherent and incoherent motions and their topologies, however the extreme requirements of statistical convergence (approximately one in 400 time steps are used for each phase angle) have made the drawing of firm conclusions concerning grid convergence impossible. For the analysis of spatial spectral content, the lack of periodicity of the flow in the box necessitates the application of window functions, however the method has been useful for examining the scales resolved by each grid, and when coupled with the phase-averaging technique, the time-dependency of these could be investigated. The snapshot POD method provides a convenient way of distinguishing space and time without any assumptions, and the indication is that at least the lower modes show relatively rapid statistical convergence.

The extent to which each method allows the issuing of concrete verdicts concerning grid convergence can however first be determined once additional data has been computed on the finest grids, which is the subject of ongoing work. Establishing the mechanism of this grid dependency and possible methods to alleviate this must also be a goal of future study.

Acknowledgements
This work was supported by the EU within the research project DESider (Detached Eddy Simulation for Industrial Aerodynamics – http://cfd.me.umist.ac.uk/desider) under contract no. AST3-CT-200-502842.

For NLR, this work was also supported under its 'Kennis als vermogen programma Platformtechnologie en flight physics' program.

The time-consuming TU-Berlin computations on the fine grid were made possible thanks to the use of the IBM pSeries 690 at the Zuse-Institut Berlin (ZIB) and the Norddeutschen Verbund für Hoch- und Höchstleistungsrechnen (HLRN), which is gratefully acknowledged.

References

1. U. Bunge, C. Mockett and F. Thiele. Calibration of different models in the context of Detached-Eddy Simulation. *AG STAB Mitteilungen*, DGLR, Göttingen, (2003).
2. R.P.Dwight, Time-Accurate Navier-Stokes Calculations with Approximately Factored Implicit Schemes. *Proceedings of the ICCFD3 Conference Toronto*, (2004)
3. D. Guenot. Simulation des effets instationnaires à grande échelle dans les écoulements décollés. PhD Thesis, SUPAERO, Toulouse, (2004).
4. W. Haase, B. Aupoix, U. Bunge and D. Schwamborn. FLOMANIA: Flow-physics modelling – an integrated approach. *Notes on Numerical Fluid Mechanics and Multidisciprlinary Design*, **94**, Springer Verlag, (2006).
5. A. Jameson. Time Dependent Calculations Using Multigrid, with Applications to Unsteady Flows Past Airfoils and Wings,textitAIAA, texbf91-1596,(1991).
6. K.C. Karki and S.V. Patankar. Pressure based calculation procedure for viscous flows at all speeds. *AIAA Journal*, **27**, 1167–1174, (1989).
7. J.C. Kok and S.P. Spekreijse. Efficient and accurate implementation of the $k - \omega$ turbulence model in the NLR multi-block Navier-Stokes system. In *Proceedings ECCOMAS 2000*, Barcelona, Spain, (2000).

8. J.C. Kok, H.S. Dol, B. Oskam and H. van der Ven. Extra-large eddy simulation of massively separated flows. In *Proc. 42nd Aerospace Sciences Meeting/Exhibit*, Reno (NV), USA, AIAA-2004-264, (2004).
9. J.C. Kok. Symmetry and dispersion-relation preserving high-order schemes for aeroacoustics and aerodynamics. In *Proceedings ECCOMAS CFD 2006*, Egmond aan Zee, the Netherlands, 2006.
10. C. Mockett, U. Bunge and F. Thiele. Turbulence modelling in application to the vortex shedding of stalled airfoils. In *Proceedings of the ERCOFTAC International Symposium on Engineering Turbulence Modelling and Measurements, ETMM6*, 617–626, Sardinia, Italy, (2005).
11. S. Obi, M. Perić and M. Scheurer. Second moment calculation procedure for turbulent flows with collocated variable arrangement. *AIAA Journal*, **29**, 585–590, (1991).
12. T. Rung and F. Thiele. Computational modelling of complex boundary-layer flows. In *9th Int. Symp. on Transport Phenomena in Thermal-Fluid Engineering*, Singapore, (1996).
13. D. Schwamborn, T. Gerhold and V. Hannemann. On the validation of the DLR Tau code. In *New Results in Numerical and Experimental Fluid Mechanics II. Contributions to the 11th AG STAB/DGLR Symposium*, W. Nitsche, H.J. Heinemann and R. Hilbig, editors, Berlin, Germany, (1998).
14. L. Sirovich, K.S.Ball, and R.A. Handler. Propagating structures in wall-bounded turbulent flows. *Theoret. Comput. Fluid Dynamics*, **2(12)**, 307-317, (1991).
15. P.R. Spalart and S.R. Allmaras. A one-equation turbulence model for aerodynamic flows, AIAA-92-0439, (1992).
16. P.R. Spalart, W.H. Jou, M. Strelets and S.R. Allmaras. Comments on the feasibility of LES for wings, and on a hybrid RANS/LES approach. In C. Lieu and Z. Liu, editors, *1st AFOSR Int. Conf. on DNS/LES*, in *Advances in DNS/LES*, Columbus, OH, Aug. 4-8, Grynden Press, (1997).
17. P.R. Spalart. Young-persons's guide to Detached-Eddy Simulation grids. *NASA contractor report* NASA/CR-2001-211032 (2001).
18. P.R. Spalart, S. Deck, M.L. Shur, K.D. Squires, M.Kh. Strelets and A. Travin. A new version of Detached-Eddy Simulation, resistant to ambiguous grid densities. For publication in *Theoretical and Computational Fluid Dynamics*, (2006).
19. K. Swalwell, J. Sheridan and W.H. Melbourne. Frequency analysis of surface pressure on an airfoil after stall. In *21st AIAA Applied Aerodynamics Conference*, (2004).
20. A. Travin, M. Shur, M. Strelets and P.R. Spalart. Detached-Eddy Simulations past a circular cylinder. *Int. J. Flow, Turbulence and Combustion*, **63**, 293–313, (2000).

21. A. Travin, M. Shur, M. Strelets and P.R. Spalart. Physical and numerical upgrades in the Detached-Eddy Simulation of complex turbulent flows. *Fluid Mechanics and its Applications*, **65**, 239–254, *Advances in LES of Complex Flows*, R. Friederich and W. Rodi, editors, (2002).
22. E. Turkel. Preconditioned methods for solving the incompressible and low speed compressible equations. *Journal of Computational Physics*, 72:277–298, 1987.
23. L. Xue. Entwicklung eines effizienten parallel Lösungsalgorithmus zur dreidimensionalen Simulation komplexer turbulenter Strömungen. PhD Thesis, Technical University of Berlin, (1998).